INFLUENCE OF Si CONTENT ON MECHANICAL PROPERTIES OF $(Ti,Zr)_{1-X}Si_XN$ MAGNETRON SPUTTERED FILMS

I.A. Saladukhin[1], G. Abadias[2], V.V. Uglov[1], S.V. Zlotski[1]

[1] Dpt. of Solid State Physics, Belarusian State University, 4 Nezavisimosti ave., 220030 Minsk, BELARUS, solodukhin@bsu.by
[2] Institut P', Université de Poitiers-CNRS-ENSMA, SP2MI, Téléport 2, F86962 Chasseneuil-Futuroscope, FRANCE, gregory.abadias@univ-poitiers.fr

Introduction

Multicomponent alloying of the transition metal nitride systems is attracting considerable interest to improve the performance of hard and wear resistant coatings. In particular, the TiZrN coatings show an enhanced hardness compared to TiN and ZrN coatings deposited under the same conditions /1-3/. It is reported that, besides higher values of hardness (>30 GPa), the oxidation resistance of TiSiN films at elevated temperatures was superior to that of TiN /4/. The formation of amorphous SiN_y interlayers at the TiN grain boundaries /4-6/ is thought to suppress the oxidation process along these high diffusive paths, thus protecting the surrounded dual-phase TiN/SiN_y structure. That is why the addition of Si into TiZrN films is considered to be perspective for their hardness and wear resistance enhancement. In the present work, the influence of the silicon content on the phase formation and mechanical properties of TiZrSiN films is investigated.

1. Preparation of thin films

TiZrSiN thin films were deposited on (001) Si substrates using reactive unbalanced magnetron co-sputtering from elemental metallic targets. Deposition was carried out at the substrate temperature T_s = 600°C in a high vacuum chamber designed by Alliance Concept. Metallic Ti (99.995% purity), Zr (99.2% purity) and Si (99.995% purity) targets were co-sputtered under $Ar+N_2$ plasma discharges. The Si content, x, in the films was varied by changing the RF power supply of the Si target from 0 up to 250 W, while maintaining the DC power supply of Ti and Zr targets constant (Table 1). The Ti and Zr target powers were chosen so as to obtain practically equal Ti and Zr concentration in the synthesized films that corresponds to the optimal Ti:Zr ratio of ternary TiZrN films which possess enhanced physical-mechanical properties. The film thickness was ~430 nm (for friction tests) and ~1 μm (for XRD analysis and hardness measurements). For the films series with the thickness of ~1 μm, the films were also deposited on the stainless steel substrates (for scratch tests).

Table 1. Process parameters and elemental composition of the magnetron sputtered TiZrSiN films at fixed working pressure (0.20 Pa), substrate temperature T_s = 600 °C and bias voltage U_s = −60 V. Grain size of c-(Ti,Zr)N solid solution extracted from XRD line broadening of (200) peak is also presented

Target power supply (W)			N_2 flow (sccm)	N_2 partial pressure (mPa)	Concentration (at.%)				Concentration ratio: Si/(Ti+Zr+Si), x	Film composition	Grain size (nm)
Ti (DC)	Zr (DC)	Si (RF)			Ti	Zr	Si	N			
250	200	–	1.1	16	22.3	25.7	–	52.0	–	(Ti,Zr)N	24
250	220	160	1.8	8.3	20.1	21.9	6.2	51.8	0.13	$(Ti,Zr)_{0.87}Si_{0.13}N$	11
250	220	200	1.9	8.4	19.1	20.7	9.5	50.7	0.19	$(Ti,Zr)_{0.81}Si_{0.19}N$	5
250	220	250	1.9	8.3	18.9	20.0	13.0	48.1	0.25	$(Ti,Zr)_{0.75}Si_{0.25}N$	5

2. Influence of Si content on phase composition of $(Ti,Zr)_{1-x}Si_xN$ films

Fig. 1 shows the evolution of XRD patterns with the rise of Si content for $(Ti,Zr)_{1-x}Si_xN$ films. It is clear that (111) and (200) peaks of c-(Ti,Zr)N solid solution are registered even at the maximum concentration of silicon (up to x = 0.25). The films structure can be described as dual-phase nanocomposite consisting of nanograins of c-(Ti,Zr)N solid solution surrounded by an amorphous SiN_y phase /7/.

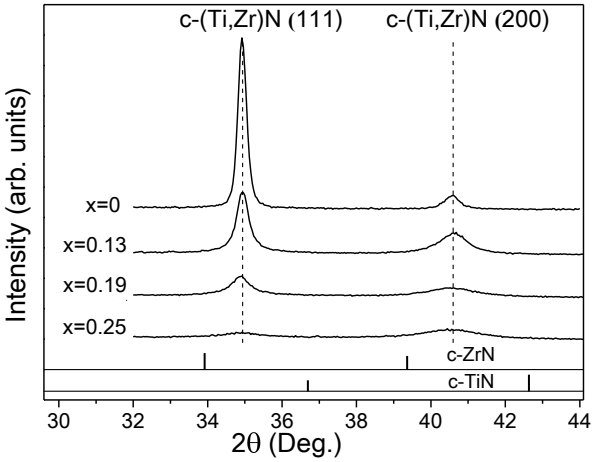

Fig. 1. XRD patterns of $(Ti,Zr)_{1-x}Si_xN$ films with different Si content, x

3. Influence of Si content on mechanical properties of $(Ti,Zr)_{1-x}Si_xN$ films

The ascertainment of the possibility of the mechanical properties optimization by means of Si adding to TiZrN film was one of the goals of the present work. Values of the hardness and Young's modulus for as-deposited $(Ti,Zr)_{1-x}Si_xN$ films are given in Table 2.

When adding silicon to TiZrN films, the hardness increases at first with Si concentration rise (up to 29.6 GPa at x = 0.13) and then it falls (Table 2). The nanocomposite structure of $(Ti,Zr)_{1-x}Si_xN$ film with x = 0.13 is already characterized by rather small size (11 nm) of c-(Ti,Zr)N solid solution grains (Table 1). At the same time the influence of the formed amorphous a-SiN_y phase on hardness is not determinative yet /7/.

Table 2. Hardness and Young's modulus of as-deposited $(Ti,Zr)_{1-x}Si_xN$ films with different composition

Film composition	Hardness (GPa)	Young's modulus (GPa)
(Ti,Zr)N	22.2±0.8	249±12
$(Ti,Zr)_{0.87}Si_{0.13}N$	29.6±1.0	278±11
$(Ti,Zr)_{0.81}Si_{0.19}N$	24.4±1.1	246±9
$(Ti,Zr)_{0.75}Si_{0.25}N$	20.5±1.3	226±11

Along with the hardness, the tribology properties of the films are important for their practical applications. The first series of measurements of the friction coefficient were made for the films deposited on the silicon substrates. Use of low load at the indenter (0.2 N) allowed to avoid coatings attrition in spite of their relatively low thickness (~430 nm). As it follows from the friction coefficient μ curves presented in Fig. 2, the nature of friction is almost identical as for (Ti,Zr)N films and for $(Ti,Zr)_{1-x}Si_xN$ films with various x. When reaching x = 0.25, the reduction of μ value to 0.23 (instead of μ~0.3 for other films) takes place. Such a reduction can be caused by the formation of more uniform microstructure of the film in the case of x = 0.25 (Fig. 3) as well as reduced elastic modulus (Table 2).

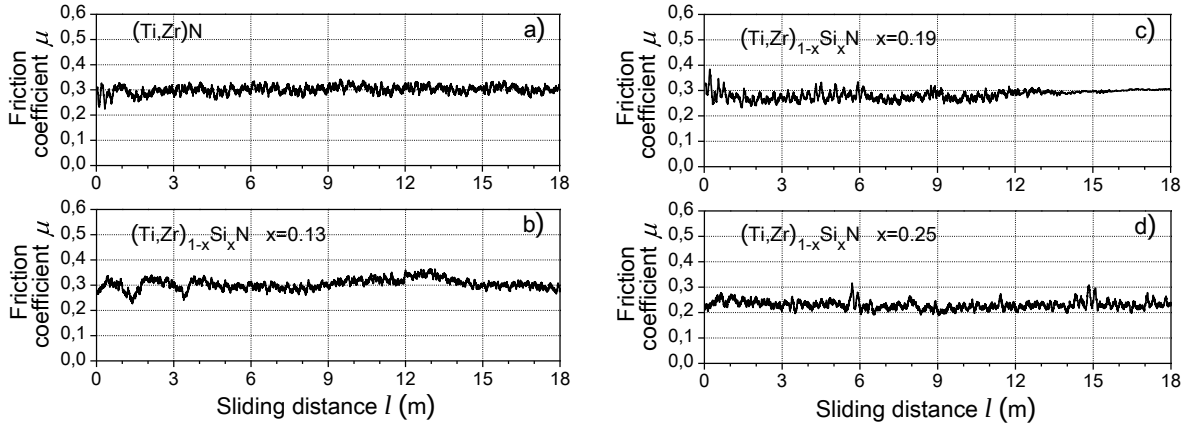

Fig. 2. Friction coefficient versus sliding distance at the reciprocation motion of the indenter on $(Ti,Zr)_{1-x}Si_xN$ films with x=0 (a), 0.13 (b), 0.19 (c) and 0.25 (d)

For the purpose of an assessment of the friction coefficient and wear resistance, the scratch tests of thicker films (thickness of 1 μm) on the steel substrates were also carried out at the continuously increasing loading value up to 20 N when indenter penetration depth significantly exceeded film thickness. Corresponding friction coefficient curves for quaternary $(Ti,Zr)_{1-x}Si_xN$ films with various Si content are shown in Fig. 4. The beneficial role of the coating is very notable even under high loadings. When rising the Si content, the friction coefficient steadily decreases. Decrease in friction coefficient with x rise can be

connected with the microstructural changes which include the reduction of the grain sizes and approach of the structure to the amorphous state (Table 1, Fig. 1). In particular, the friction coefficient for the sample with $(Ti,Zr)_{1-x}Si_xN$ film (x = 0.25) is 1.5 times less than for the sample with (Ti,Zr)N film at the loading value of 10 N (Fig. 4).

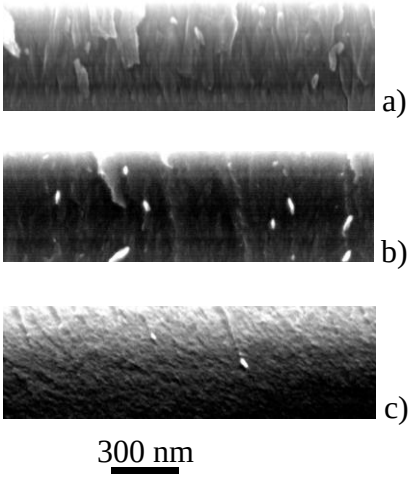

Fig. 3. Cross-sectional SEM micrographs of $(Ti,Zr)_{1-x}Si_xN$ films with x=0 (a), 0.13 (b), 0.25 (c)

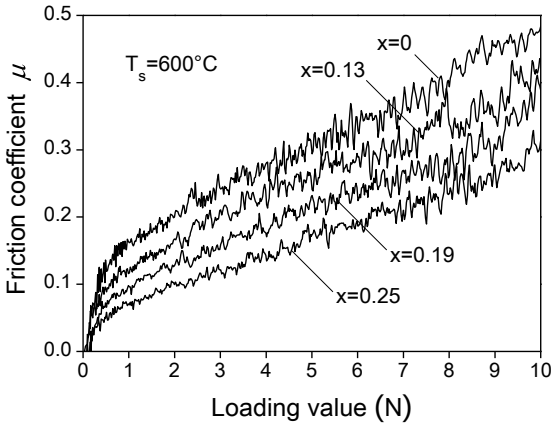

Fig. 4. Dependence of friction coefficient on loading value for $(Ti,Zr)_{1-x}Si_xN$ films with different Si content

Conclusions

For magnetron sputtered $(Ti,Zr)_{1-x}Si_xN$ films ($0.13 \leq x \leq 0.25$) the dual-phase structure is formed: the nanocomposite on the basis of c-(Ti,Zr)N solid solution and the grain-boundary amorphous a-SiN_y phase. The maximum hardness value (29.6 GPa) is observed when Si content x = 0.13. $(Ti,Zr)_{1-x}Si_xN$ films with higher Si content are characterized by lower friction coefficient especially in the case of coating deposition onto the steel substrates.

References

1. **PalDey S., Deevi S.C.** Mater. Sci. Eng., A342 (2003) 58–79.
2. **Lin Y.-W., Huang J.-H., Yu G.-P.** Thin Solid Films, 518 (2010) 7308–7311.
3. **Uglov V.V., Anishchik V.M., Khodasevich V.V., Prikhodko Zh.L., Zlotski S.V., Abadias G., Dub S.N.** Surf. Coat. Technol., 180–181 (2004) 519–525.
4. **Jiang N., Shen Y.G., Mai Y.-W., Chan T., Tung S.C.** Mater. Sci. Eng., B106 (2004) 163–171.
5. **Hu X., Han Z., Li G., Gu M.** J. Vac. Sci. Technol., A 20(6) (2002) 1921–1926.
6. **Kim S.H., Kim J.K., Kim K.H.** Thin Solid Films 420–421 (2002) 360–365.
7. **Saladukhin I.A., Abadias G., Michel A., Uglov V.V., Zlotski S.V., Dub S.N., Tolmachova G.N.** Thin Solid Films, 581 (2015) 25–31.